Transconductance Power Amplifier Systems for Current-Driven Loudspeakers

Article *in* Journal of the Audio Engineering Society · October 1989

CITATIONS
8

READS
902

2 authors, including:

Malcolm John Hawksford
University of Essex
235 PUBLICATIONS **1,208** CITATIONS

SEE PROFILE

Transconductance Power Amplifier Systems for Current-Driven Loudspeakers*

P. G. L. MILLS

Tannoy Limited, Coatbridge, Strathclyde ML5 4TF, UK

AND

M. O. J. HAWKSFORD

University of Essex, Wivenhoe Park, Colchester, Essex, CO4 3SQ, UK

Moving-coil loudspeakers generally provide a substantial improvement in linearity when current driven, together with the elimination of voice-coil heating effects. Consequently there is a need to investigate low-distortion power amplifier topologies suitable for this purpose. After considering established current feedback approaches, a novel method using a common-base isolation stage is outlined and extended to show a prototype amplifier circuit in detail. In addition, the elements of a two-way active current-driven system are described, with low-frequency velocity feedback control derived from a sensing coil. The coupling error between this coil and the main driving coil is nulled by electronic compensation.

0 INTRODUCTION

The moving-coil drive unit can readily be shown to benefit in terms of linearity when controlled by a current source rather than the more conventional voltage source. Throughout this paper we will term this mode of operation *current drive*, whereby the amplifier source impedance can, to all intents and purposes, be considered infinite compared to the drive unit impedance.

Of the drive unit error mechanisms that can be countered by current drive, the voice-coil resistance is of particular interest. As a result of self-heating in excess of 200°C, the increase in coil resistance leads to sensitivity loss (often referred to as power compression [1], [2]), loss in electrical damping of the fundamental resonance, and crossover filter misalignment. In their paper Hsu et al. [3] concluded that a satisfactory method of compensating for the effect had yet to be found.

At higher frequencies, nonlinearity occurs as the coil inductance is modulated by movement in the magnetic circuit and by other effects such as magnetic hysteresis [4]. Measurements under current drive have shown, in comparison with voltage drive, a high-frequency distortion reduction of typically 20–30 dB for a bass–midrange drive unit.

These performance advantages arise from the coil resistance and inductance being totally eliminated from the system transfer function. The force on the cone is proportional to the voice-coil current, not the applied voltage. Analysis also shows a reduced dependence on nonlinearity within the force factor and mechanical impedance of the drive unit.

Thus as a result of the performance gains that can be demonstrated using current drive, there arises the need to investigate suitable power amplifier topologies to make the best of the technique. This paper therefore aims to review some of the earlier published work on transconductance amplifier design, while presenting new topologies and detailed circuitry of a two-way active prototype system. In addition, due to the loss of voice-coil damping under current drive, control circuitry for restoring damping by means of motional

* Manuscript received 1988 July 6. This paper expands on some areas covered by the authors in "Distortion Reduction in Moving-Coil Loudspeaker Systems Using Current-Drive Technology," volume 37, number 3 (1989 March).

feedback applied to the bass–midrange drive unit is described, along with the low-level crossover circuitry of the prototype system.

1 POWER AMPLIFIER TOPOLOGIES FOR CURRENT DRIVE

1.1 Review of Transconductance Amplifier Techniques

A transconductance power amplifier requires a high output impedance that is linear and frequency independent. It must also possess the attributes of a conventional voltage power amplifier such as high linearity, wide bandwidth, freedom from slewing-induced errors, and insensitivity to load variations (be they linear or nonlinear).

The most commonly used technique to obtain a high output impedance is to apply current feedback around a conventional power amplifier by means of a sensing resistor in the loudspeaker earth return [5], [6], as illustrated in Fig. 1. The transconductance g_m is defined

$$g_m = \frac{1}{R_f} . \quad (1)$$

The method has also been used in high-current industrial applications. There are two main disadvantages with such a system. First, the open-loop gain of the amplifier is frequency dependent as a result of the amplifier's dominant pole, and this is reflected in the output impedance. Second, the loudspeaker impedance, which is both frequency dependent and nonlinear, tends to modulate the transconductance of the amplifier. The fact that the load is not ground referenced may be considered inconvenient in some applications.

A refinement of the basic technique was described in Lewis [7]. The circuit was symmetrical in nature, using two current-sensing resistors, with a ground referenced load fed from MOSFET output devices. Good linearity was indicated at 10-W average power into a 5-Ω load. However due to class A operation, the design would be inefficient at the power levels necessary for a moving-coil drive unit (between 50 and 100 W typically). Care must be taken to minimize output offset current with this scheme.

A further ground-referenced current feedback scheme was described in Nedungadi [8], but this required the complexity of a differential voltage-to-current converter in conjunction with a floating sensing resistor in order to maintain current feedback.

Another technique used in implementing transconductance amplifiers involves the combination of supply current sensing around a follower, together with current mirrors feeding the load [9]. The arrangement is shown in Fig. 2, where R_f is a dummy load and the transconductance is again defined by Eq. (1). Operation of the circuit is typically in class AB.

While suitable for low output currents (<50 mA peak), the approach is difficult to extend to the levels required for driving a loudspeaker (typically 5 A peak or more) due to the linearity of the mirrors and also power loss in R_f. Although the mirrors could be arranged to provide current gain and could be partially linearized by error-correction techniques [10], the technique is not felt to offer a particularly practical solution.

1.2 Methods Using a Common-Base Isolation Stage

The approach devised to overcome the limitations cited as being inherent to existing topologies is illustrated in basic form by Fig. 3. The notable aspect of this strategy is the open-loop grounded base stage, which isolates the load Z_L from the main amplifier A_t while providing a naturally high output impedance without the use of overall current feedback. In addition a cascode configuration is formed in conjunction with the output devices in the main amplifier A_t. Resistor R_f defines the transconductance, driven from amplifier A_t, a voltage source, which may operate with low values of supply voltage $\pm V_{SI}$ to reduce power dissipation. The loudspeaker is referenced to ground and isolated from any feedback loop used to linearize the amplifier A_t. Although a successful prototype based on this scheme has been constructed, with amplifier A_t running in class A and with a class AB output stage, it is to some extent an uneconomical solution due to the need for two pairs of floating power supplies.

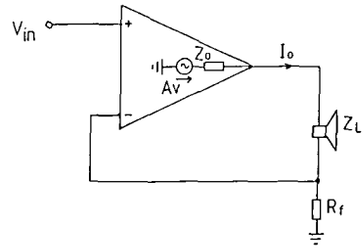

Fig. 1. Basic current-feedback-derived transconductance amplifier.

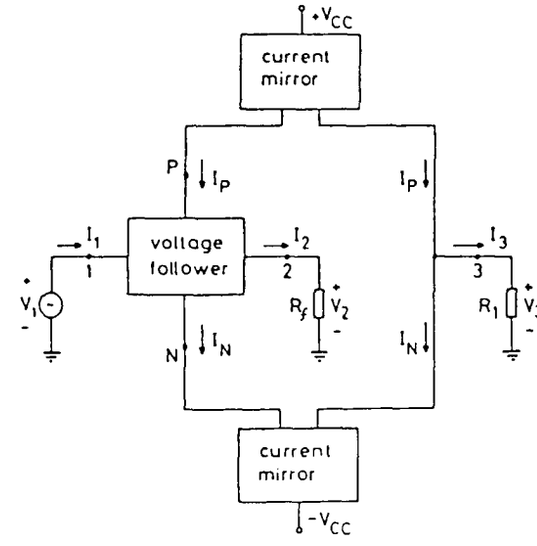

Fig. 2. Voltage-current converter. After Rao and Haslett [9].

A more viable alternative is the revised topology illustrated by Fig. 4. This circuit takes the form of a current amplifier of current gain

$$\alpha = -\frac{R_x}{R_f} \tag{2}$$

The first-stage power supply $\pm V_{S1}$ is ground referenced, unlike the previous case, meaning that several power amplifiers within an active system may share a common supply, thus reducing complexity and cost. Like the previous scheme, the current flowing in the transconductance defining resistor R_f is that which flows in the load Z_L, except for any base current lost to ground in the common-base stage. The fact that the amplifier A_i is referenced to the input of the common-base stage and not to ground tends to decouple it from any distortion appearing at the emitters of the common-base stage.

This topology forms the basis of the prototype system, the detailed circuitry of which is described in Sec. 2. On a practical note, it is important to provide adequate current gain in the common-base stage in order to prevent nonlinear current loss to ground, which introduces distortion.

1.3 Alternative Approaches

All of the circuits described so far rely on a current-sensing resistor to define the overall system transconductance. Even when this resistor is of a low value (about 1 Ω), it still tends to dissipate an appreciable amount of power. This element would at first seem to be fundamental to the design of a transconductance amplifier, but it is interesting to note the possibilities of transformer-derived feedback in perhaps reducing such losses.

Nordholt, in his classification of feedback configurations [11], described how transformer-derived feedback could be used to generate transconductance and current gain functions, as shown in Fig. 5. In Fig. 5(a) resistor R_f is still necessasry in order to define the stage transconductance.

Although no research has been directed in this area and the approach is only conceptual in nature, it may be worth further investigation, given a wide-bandwidth transformer design.

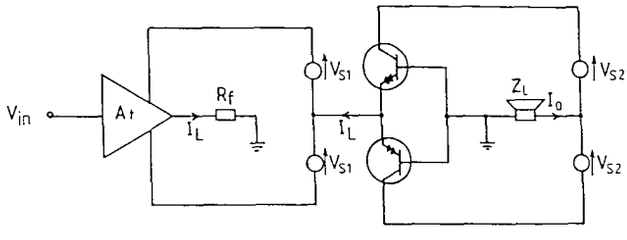

Fig. 3. Basic transconductance power amplifier using grounded-base output stage.

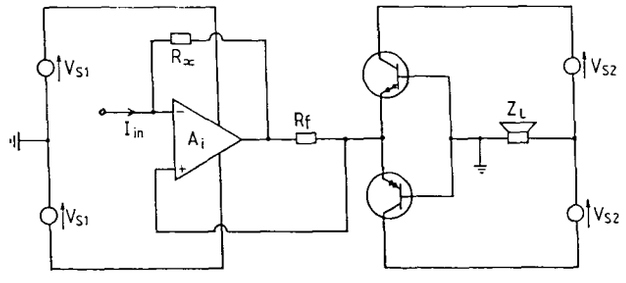

Fig. 4. Alternative configuration for current gain.

2 PROTOTYPE AMPLIFIER SYSTEM

2.1 General Overview

The two-way active loudspeaker system constructed to validate the basic approach proposed for high output impedance power amplifier design was based on the Celestion SL600 loudspeaker. In this section the current gain power amplifier is considered in detail along with the necessary transconductance preamplifier, while Sec. 3 considers the associated motional feedback control circuitry, which is required for the bass–midrange drive unit.

Throughout the design, the underlying philosophy has been to use symmetrical direct-coupled circuitry to give good transfer function linearity without recourse to high levels of overall negative feedback [12], [13]. DC stability is taken care of by servo amplifiers (feedback integrators).

2.2 Transconductance Preamplifier

Fig. 6 shows a two-stage design, the basic topology of which has often been used with overall feedback as

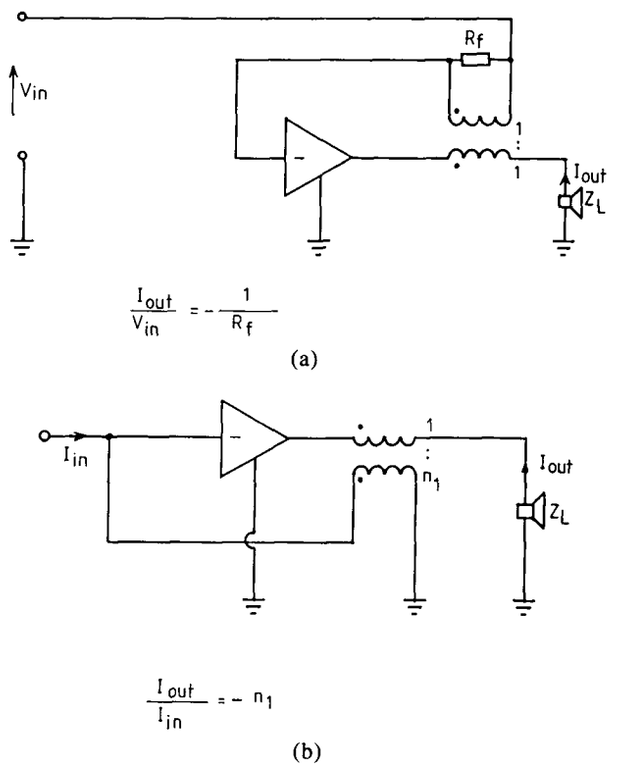

Fig. 5. Transformer-derived feedback systems. After Nordholt [11]. (a) Transconductance stage. (b) Current gain stage.

a voltage gain stage [14]. It is operated here open loop to provide a high output impedance and consequently must be capable of good linearity.

Transistor pairs Q_3/Q_4 and Q_5/Q_6 form cascodes to increase high-frequency linearity and give a high output impedance. Bias arrangements for the cascode are somewhat unusual in that resistors R_{14} and R_{15} are not returned to the supply rails, but are connected to the emitters of the common-emitter part of the cascode, thus avoiding nonlinearity from base current loss in the common-base devices [15]. This reduces high-frequency distortion by typically a factor of 10 at 20 kHz over the conventional bias method.

Operational amplifier IC_1 with associated passive components forms a current-sensing differential servo amplifier to null any output offset current due to imbalances in the main circuit and has no effect on performance within the audio band. This configuration of servo amplifier, to the authors' knowledge, has not been seen before in the literature.

At frequencies within the passband of the amplifier, the transconductance g_m may be approximated by the expression

$$g_m = \frac{I_{out}}{V_{in}} \approx \frac{R_6}{R_{11}(R_8/2 + R_{10})} . \quad (3)$$

With the component values shown, $g_m \approx 4$ mS.

In addition to the main input and output, an auxiliary velocity feedback input is provided along with an error-nulling output. These are only required for low-frequency use, and their function is described in Sec. 3 when considering the velocity feedback control circuitry.

2.3 Current Gain Power Amplifier

The current gain power amplifier, which accepts the output of the transconductance preamplifier, is based on the structure shown in Fig. 4. For the purpose of description, it is split into three sections: input amplifier, power follower, and common-base output stage. Both input amplifier and follower are represented by the gain block A_i in this simplified representation.

We consider first the input amplifier, Fig. 7. This is essentially the same topology as the transconductance preamplifier, but with a few refinements. Input stage biasing is performed with current sources based around transistors Q_1 and Q_2, instead of resistive biasing. This is a result of the need to provide immunity to the greater level of supply rail contamination caused by class AB operation of the power follower stage. The output from the transconductance preamplifier is fed to the emitters of the input devices Q_3 and Q_4, which thus operate in common-base mode. The first and second stages of the amplifier are coupled together by current mirror pairs Q_5/Q_8 and Q_9/Q_{12} to reduce loading effects and interaction between the two stages. These mirrors are themselves linearized by local error feedback correction consisting of transistor pairs Q_6/Q_7 and Q_{10}/Q_{11}. This approach has been previously documented [10], al-

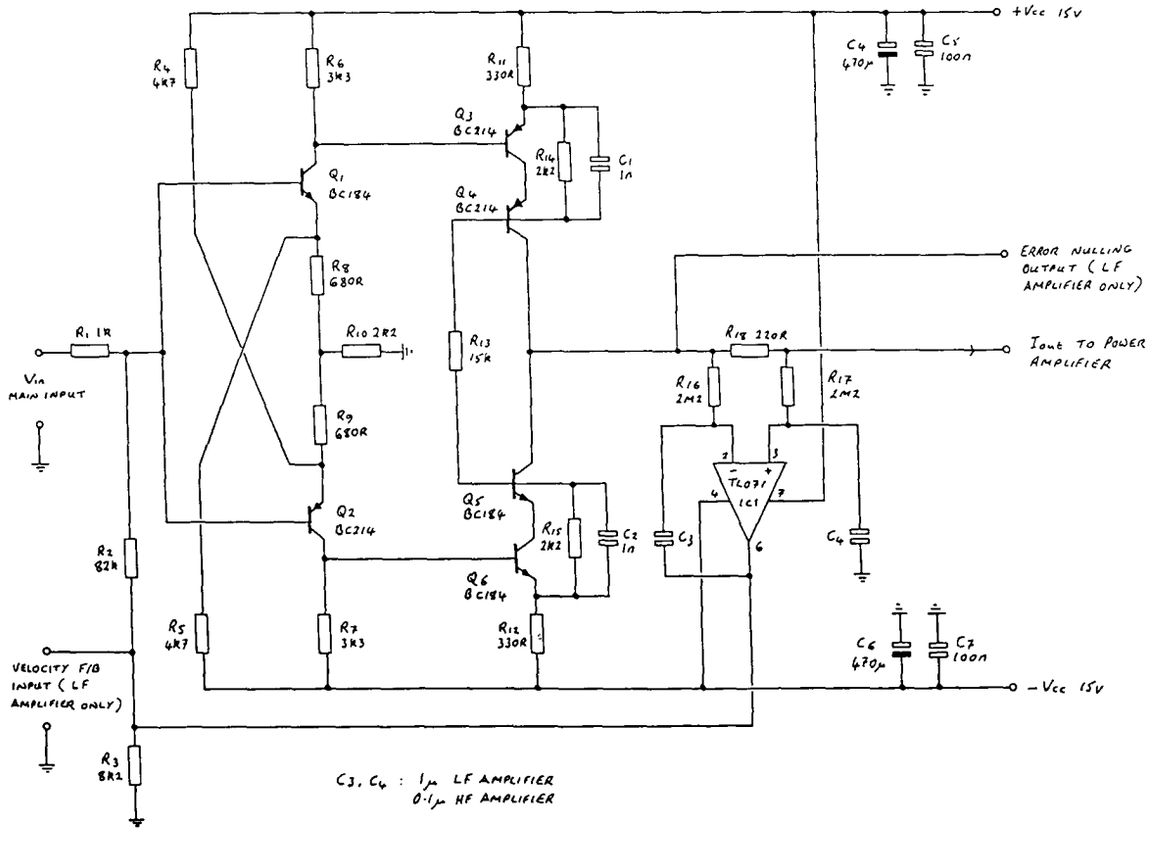

Fig. 6. Transconductance preamplifier.

though in this case some current gain has been introduced into the mirrors to enable correct quiescent operating conditions to be established in the first and second gain stages.

The outputs from the cascode pairs Q_8/Q_{13} and Q_{12}/Q_{14} are displaced ± 4 V about ground by green LEDs D_1–D_4, in order to bias the next stage. Resistor R_{28} and capacitor C_3 are included to define the open-loop gain characteristics of the amplifier, to ensure that stability is maintained under closed-loop conditions.

Fig. 8 shows the next section, which is a follower with extensive error-correction circuitry and is essentially similar to a previously published topology [16], but with improvements to biasing arrangements. It is worth briefly reviewing the principle of operation.

Transistor pairs Q_{16}/Q_{18} and Q_{17}/Q_{19} form a Darlington follower, preventing loading of the previous stage and driving the Darlington output devices Q_{30} and Q_{31}. Transistors Q_{28} and Q_{29} form V_{be} multipliers to bias the output Darlingtons, but are also configured as error amplifiers, which together with Q_{22} and Q_{23} form the main error feedback loop, delivering a correction current through resistors R_{38} and R_{78} in response to any nonlinearity in the output devices Q_{30} and Q_{31}. R_{48} is included as an adjustment to achieve the best distortion null.

In order to linearize Q_{18} and Q_{19}, which have to drive the output Darlingtons, additional error correction in the form of feedforward is applied with the aid of Q_{20} and Q_{21}, in combination with the input transistors Q_{16} and Q_{17}. Further linearization is achieved by current mirror transistors Q_{25} and Q_{26}, which form a negative feedback loop, thus reducing the source impedance seen by output Darlingtons Q_{30} and Q_{31}.

Moving now to Fig. 9, which shows the output common-base stage, the preceding follower drives current through resistor Q_{67}, which in conjunction with R_2 (Fig. 7) sets the midband current gain of the complete amplifier to around 800. Inductor L_2 serves to reduce the high-frequency current gain of the amplifier to ensure stability. The current in R_{67} flows into the common-base output stage, consisting of Darlingtons Q_{32} and Q_{33}, along with driver devices Q_{36} and Q_{37}, the bases of which are referenced to ground. Except for any current loss to ground, such as through the bases of these devices and through the biasing current sources (Q_{34}, Q_{35}), the current in R_{67} flows through the load via floating power supplies $\pm V_{CC2}$.

In order to establish a low-output offset current for the amplifier (typically less than ± 2 mA), a servo based around IC_1 and referenced to the input of the common-base stage, is used to feed a dc compensation current back to the input of the amplifier.

To prevent switch-on and switch-off transients from reaching the load, relay RL_1 is included, controlled by a time-delay circuit on startup and almost instantaneously dropping out on power down. The control circuitry to perform this function is not shown.

The power amplifier together with the transconductance preamplifier was evaluated in terms of standard

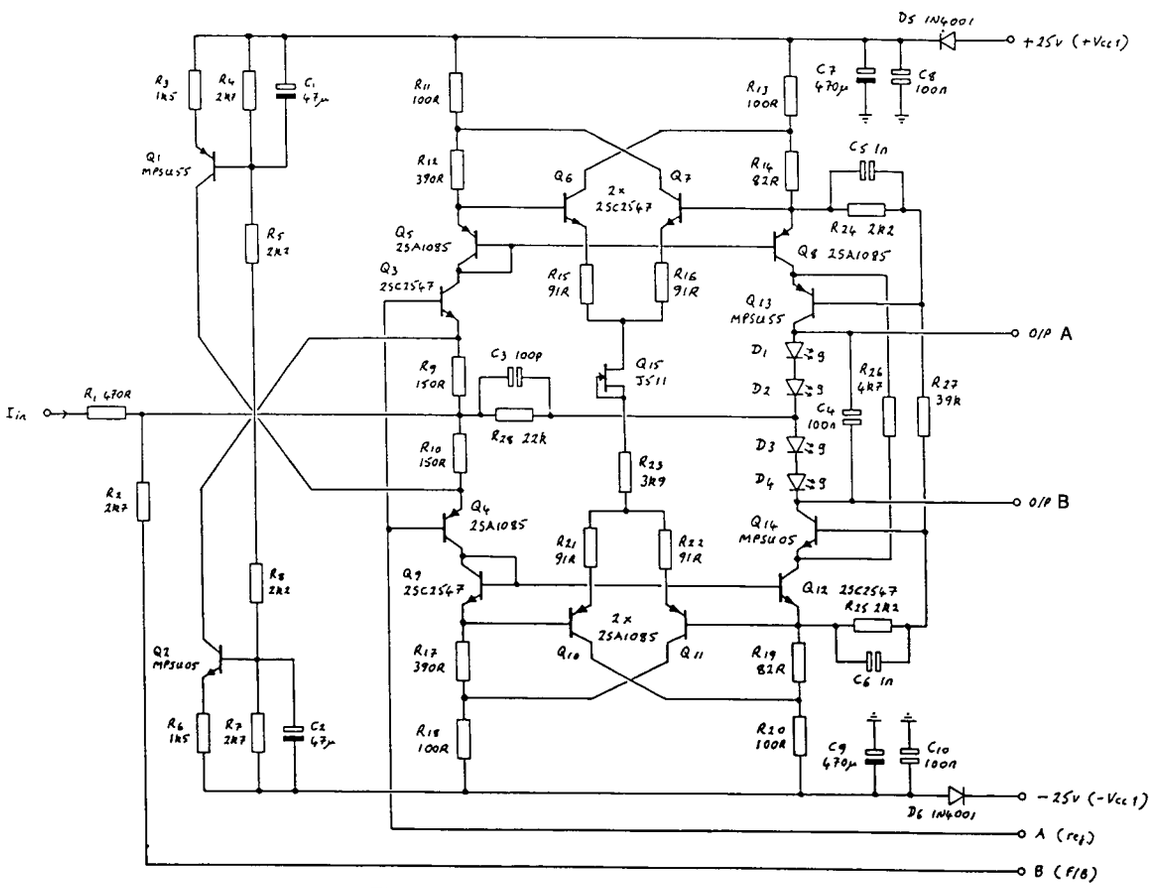

Fig. 7. Prototype amplifier, input stage.

measurements and found to be comparable with a typical high-performance conventional amplifier. The results are as follows:

Rated power output (8-Ω resistive load)	75 W average
Total harmonic distortion at rated power	
20 Hz	−79 dB
1 kHz	−86 dB
20 kHz	−68 dB
Intermodulation distortion (19 and 20 kHz at equal levels at rated power)	−86 dB
Hum and noise (re maximum output)	−90 dB
Small-signal bandwidth, −3 dB	0.1 Hz to 50 kHz
Output impedance*	
20 Hz	4.1 MΩ
1 kHz	106 kΩ
20 kHz	11.4 kΩ

* From computer simulation, due to the difficulty in performing these measurements.

It is interesting to note that the distortion measurements may only easily be made indirectly by converting the output current to a voltage, by means of a resistive load bank. The measurements as shown will thus reflect any nonlinearity in the load.

The protective features, consisting of output fuses and relay contact, should not introduce any degradation in performance, as they are in series with a high source impedance, which is not the case with a conventional power amplifier.

3 VELOCITY FEEDBACK CONTROL SYSTEM

3.1 Outline Approach

In order to compensate for the loss in electric damping of the bass–midrange unit caused by the high amplifier output impedance, velocity feedback was used to restore damping [5], [6]. While many forms of sensing arrangement have been described ([17]–[23], for example), the method adopted here is attractive for reasons of mechanical simplicity and cost effectiveness. The technique used is to wind a sensing coil over the main voice coil of the drive unit. The output voltage of the sensing coil will ideally be defined by

$$V_s = (Bl)_s u \tag{4}$$

where $(Bl)_s$ is the sensing coil Bl product, N/A, and u is the cone velcity, m/s.

Unfortunately an error is induced in the sensing coil by transformer action from the main driving coil. In the previously documented work induced errors were overcome by neutralizing coils or by an altogether more elaborate mechanical arrangement to physically isolate the driving and sensing coils. With the approach considered here, a procedure of electronic compensation has been chosen in order to avoid expensive tooling costs for a specialized drive unit.

The physical arrangement of the assembly is shown in Fig. 10. It should be noted that in this case, the sensing coil follows roughly the same Bl profile as the main driving coil, so the action of velocity feedback

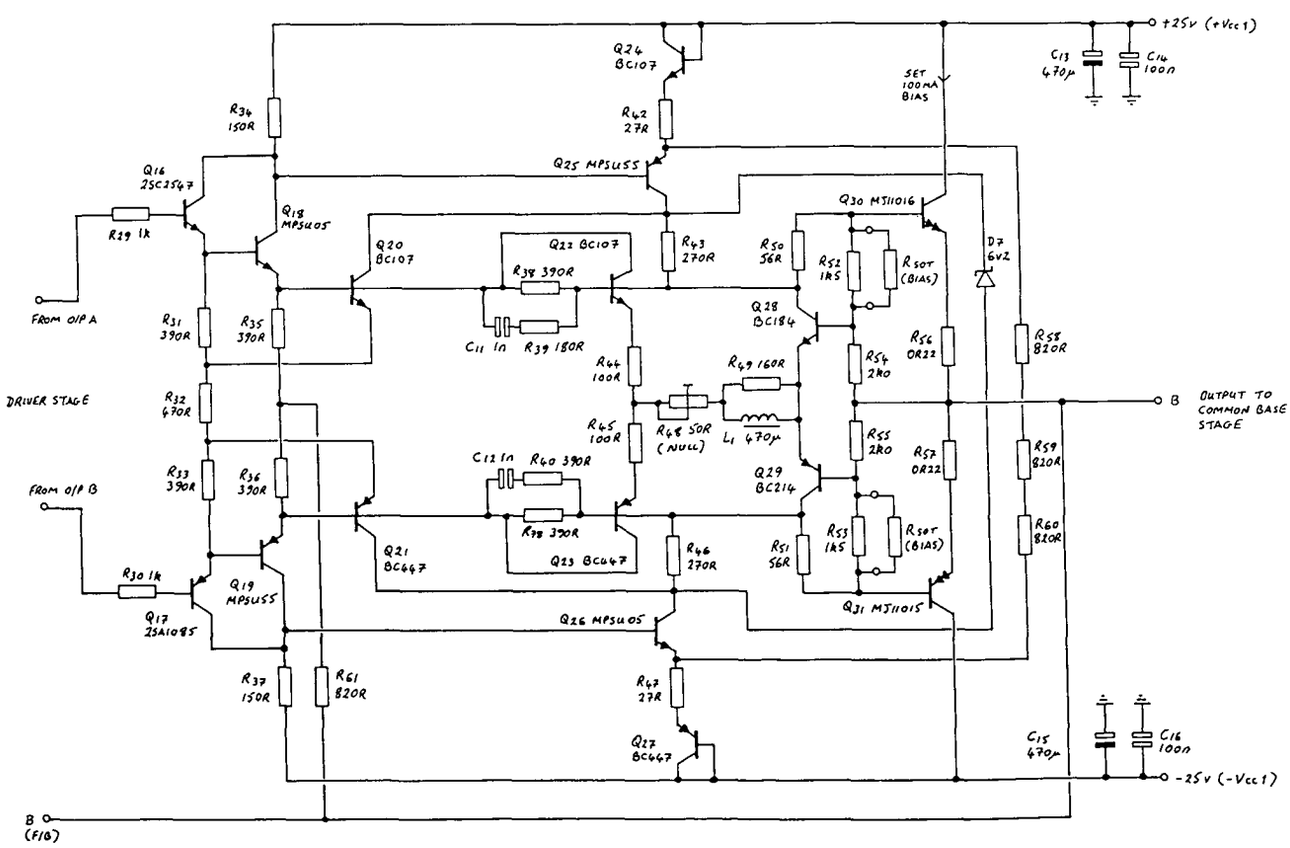

Fig. 8. Prototype amplifier, follower stage.

does not improve linearity above that already afforded by the current drive.

If a longer sensing coil could be accommodated (or indeed a very short coil that remained well within the magnet gap), a further reduction in distortion would be possible.

3.2 Coupling Error Compensation

In order to investigate the nature of the transformer coupling error, Fig. 11 shows the error magnitude with respect to frequency for the coil assembly at equilibrium and also at both extremes of travel. For this measurement the driving coil was powered from the prototype transconductance amplifier system. The level of error is seen to be frequency dependent, rising initially at a rate of approximately 4.6 dB/octave. This unusual characteristic is considered to be a function of pole-piece coupling with the magnetic circuit, but a full analysis of the mechanisms at work has not been undertaken. In addition, some positional dependence of the error magnitude is also apparent. At 100 Hz the coupled error is around 15 dB below the voltage appearing on the driving coil, thus illustrating the need for an effective compensation system.

To implement the compensator, it is necessary to derive a signal proportional to the current in the driving coil and to subject this signal to the same frequency dependence as the error mechanism itself in order to null the error from the sensing coil output. The variation in error level with displacement (typically ± 3 dB) has not been accounted for.

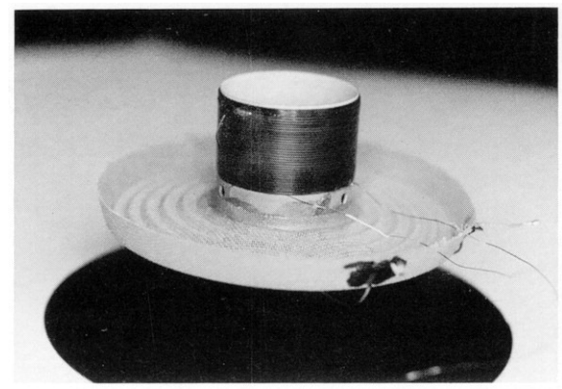

Fig. 10. Sensing-coil assembly.

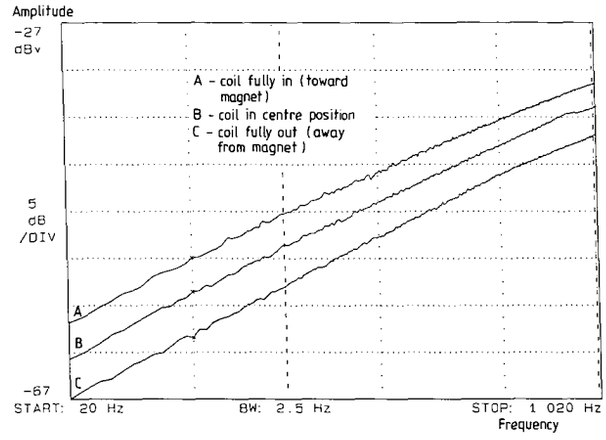

Fig. 11. Measured transformer coupling error.

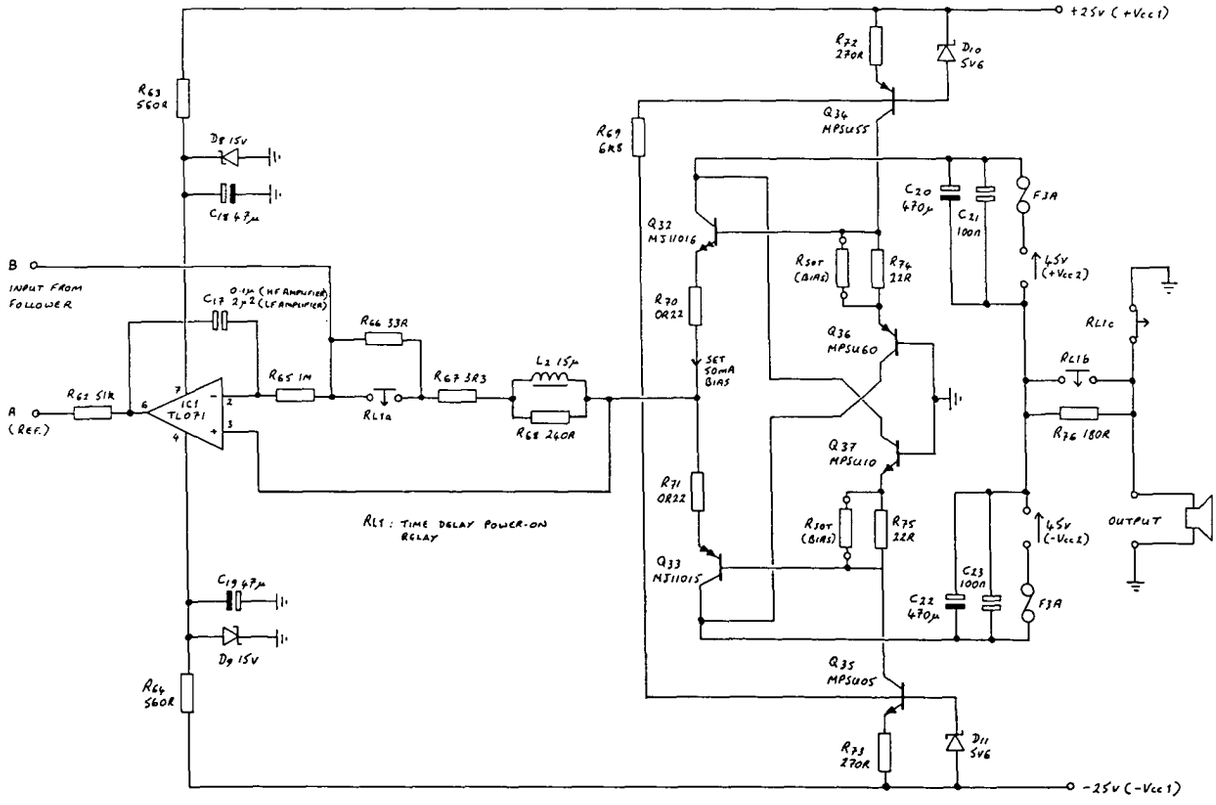

Fig. 9. Prototype amplifier, common-base stage. Protection relay contacts RL_1 are shown with amplifier shut down.

Fig. 12 illustrates the general approach to synthesis of the frequency-dependent element of the compensator. A number of first-order sections are combined, with pole–zero locations set to produce a slope approximating that desired. The general circuit configuration to give this response is shown in Fig. 13 for an nth-order compensator. The transfer function of this circuit is written

$$\frac{V_{out}}{V_{in}} = -\sum_{r=0}^{n}\left(\frac{j\omega RC_r}{1 + j\omega R_r C_r}\right) . \quad (5)$$

A software optimization routine was used to select component values in order to match the 4.6-dB/octave slope required. For a 6th-order compensator, the computer-predicted frequency response is shown in Fig. 14, which also lists the nearest preferred value component values chosen. The result is deemed more than adequate for our purposes, bearing in mind that some positional dependence of the coupling error is present, together with a gradual deviation from the idealized 4.6-dB/octave response with increasing frequency.

3.3 Complete Control System

We continue by considering the complete velocity feedback control system shown in Fig. 15. The sensing coil (source impedance 28 Ω) is connected to a high input impedance buffer stage IC_{2a} via an attenuator network to avoid overload. IC_{2b} forms a summing amplifier in order to subtract the signal derived from the coupling error compensator.

The compensator input is differential, accepting the voltage across the servo current-sensing resistor R_{18} of the transconductance preamplifier (Fig. 6). Thus the input to the compensator is proportional to the drive unit current. This differential signal is converted to single-ended format before the 4.6-dB/octave weighting is applied by the circuitry based around IC_{1d}. R_{22} provides an adjustment to enable the best error null to be obtained with a static motor coil assembly connected to the velocity feedback input.

In order to maintain stability of the closed-loop system, a second-order low-pass filter at 500 Hz is included in the feedback control loop. This also has the benefit of reducing any residual transformer coupling error at high frequencies, where the compensator is no longer as effective due to the changing slope of the error. Finally the output of the controller is summed with the main signal at the velocity feedback input of the transconductance preamplifier, with R_{27} (Fig. 15) providing an adjustment of the low-frequency Q alignment.

To illustrate the performance of the velocity feedback control system, a number of frequency and time domain measurements were obtained. First, Fig. 16(a) shows

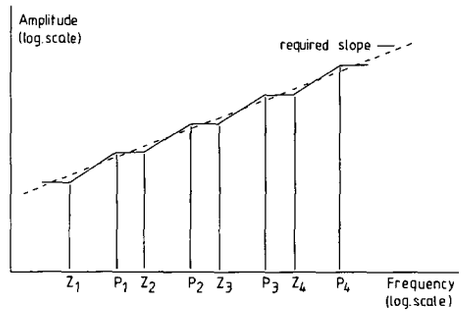

Fig. 12. Basis for synthesis of coupling error compensator.

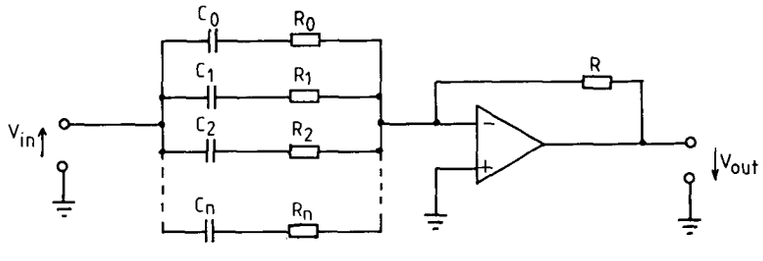

Fig. 13. General configuration for nth-order compensator.

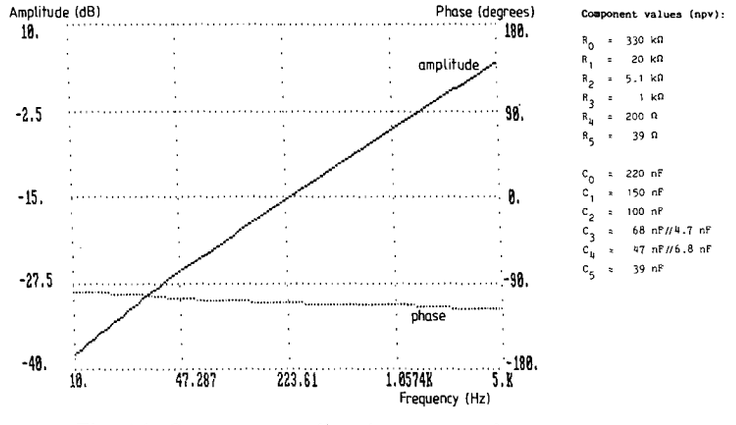

Fig. 14. Computer-predicted response of compensator.

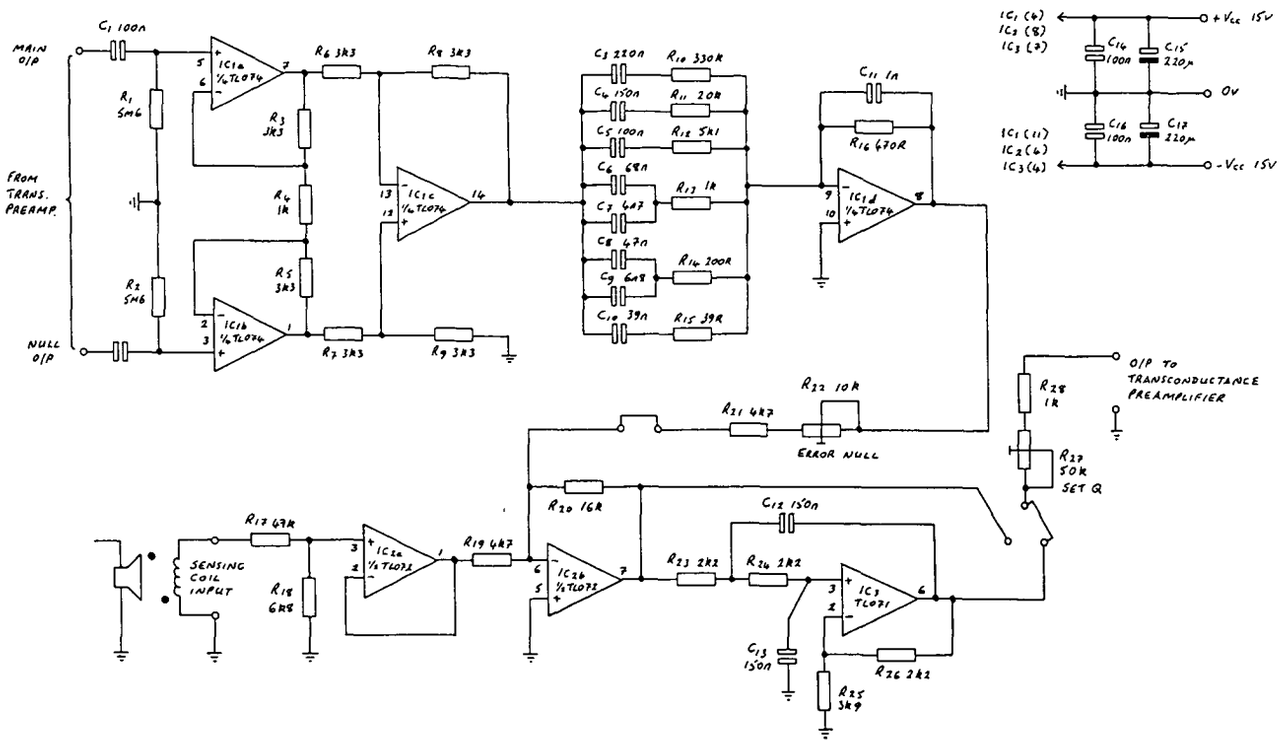

Fig. 15. Velocity feedback control system.

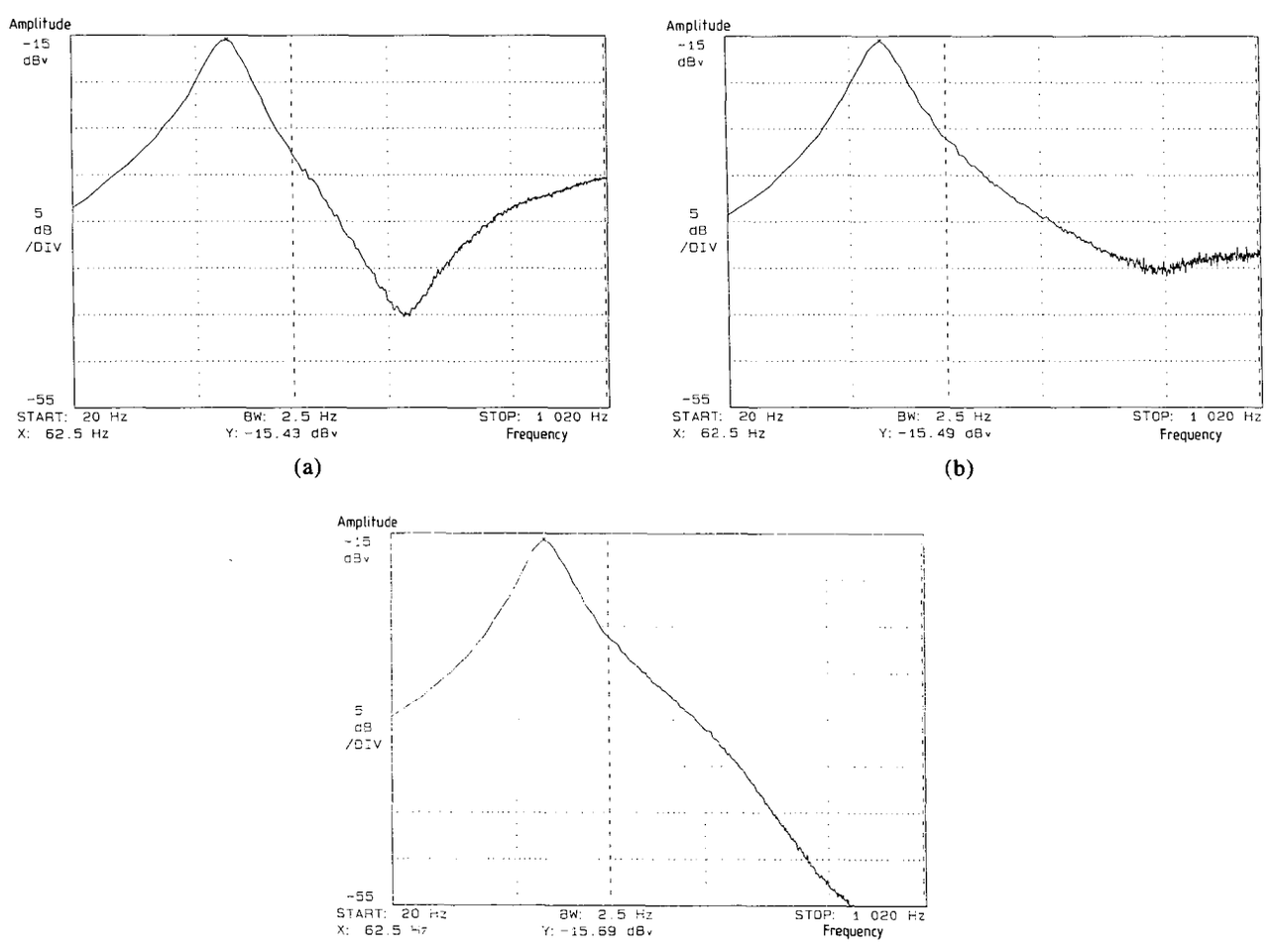

Fig. 16. Velocity feedback control signal. (a) Sensing-coil output voltage. (b) Addition of compensator. (c) Addition of compensator and low-pass filter.

the output of the sensing coil, corresponding to velocity, with frequency. The peak at 62.5 Hz corresponds to the drive unit–enclosure fundamental resonance, while the rising high-frequency output is due to the coupling error between drive and sensing coils. Fig. 16(b) shows the addition of the coupling error compensator, giving a much reduced spurious high-frequency output. The further addition of the second-order low-pass filter at 500 Hz gives the response of Fig. 16(c), which is close to an idealized velocity function.

Steady-state sine-wave measurements of the acoustic output suggest a worthwhile improvement in linearity of the bass–midrange drive unit compared to voltage drive. The following acoustic distortion measurements at a drive current of 1 A peak are illustrative:

	Voltage Drive (dB)	Current Drive* (dB)
Total harmonic distortion at 100 Hz re fundamental	−34.1	−43.3
Total harmonic distortion at 3 kHz re fundamental	−28.4	−55.0

* Under closed-loop conditions.

The effectiveness of the coupling error compensator and filter is confirmed by the fact that no increase in harmonic distortion is measurable up to 3 kHz and beyond (that is, over the full operating range of the drive unit) when the feedback loop is closed. The actual increase in distortion level present on the unfiltered and uncompensated velocity signal, compared to the drive unit acoustic output, ranges from 11 to 23 dB as frequency is increased from 500 Hz to 3 kHz.

The ability to vary the system Q with the velocity feedback control circuit is shown by means of near-field acoustic step response measurements. Fig. 17(a) is without the velocity feedback operational, showing a Q of around 2.5, which is the natural mechanical Q of the drive unit. Fig. 17(b)–(e) shows compensated Q alignments of 1.5, 1.0, 0.7, and 0.5, respectively. A value of $Q = 0.7$ preserves the low-frequency characteristics of the unmodified loudspeaker under voltage drive.

4 LOW-LEVEL CROSSOVER

To complete the two-way prototype system, a second-order low-level high- and low-pass crossover was included to integrate the drive units together, with a nominal crossover point of 3 kHz.

The crossover is implemented by passive RC elements, the time constants of which are individually adjustable to give the flattest frequency response, with buffer amplifiers between stages, to avoid loading effects. The complete system is shown in modular form by Fig. 18. After the input level control, amplifier A_1 provides a low-impedance drive to the first low- and high-pass filters, which are buffered by amplifiers A_2 and A_3 before the second set of filter sections. A_4 and A_5 are the transconductance preamplifiers previously

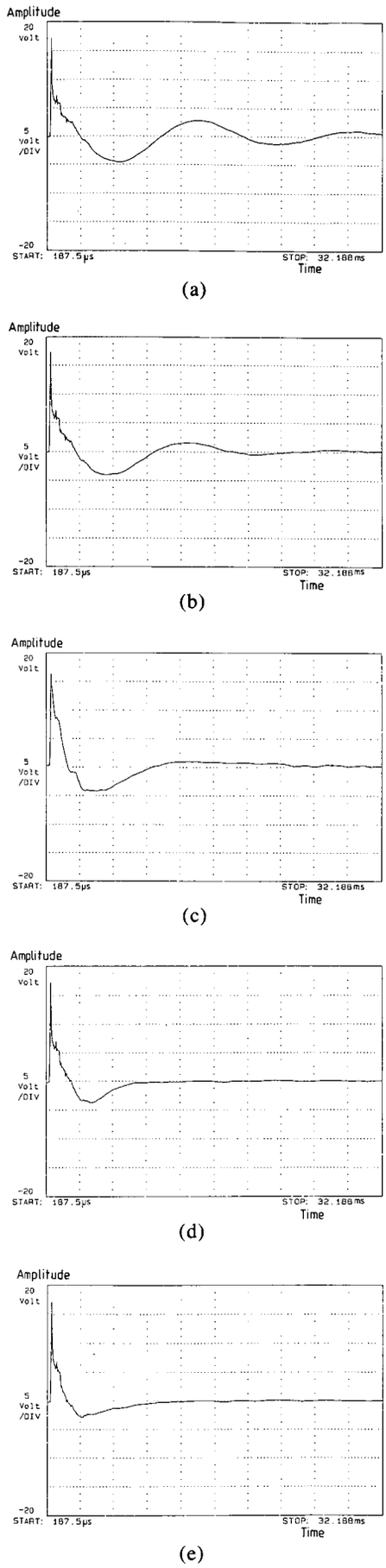

Fig. 17. Measured step responses of bass–midrange drive unit. (a) $Q = 2.5$ (no feedback). (b) $Q = 1.5$. (c) $Q = 1.0$. (d) $Q = 0.7$. (e) $Q = 0.5$.

described, which drive the high- and low-frequency power amplifiers, respectively.

The circuit topology of buffer amplifiers A_1, A_2, and A_3 (Fig. 19) is similar to the transconductance preamplifier, but with the addition of an output follower and overall negative feedback to provide a low output impedance. Certain gain and frequency response defining components are specific to individual amplifier stages as indicated.

The performance of the system is shown by the in-room measured frequency response curve of Fig. 20, with the measurement microphone 1 m on axis. The uneven high-frequency response is a function of the tweeter characteristics, with the resonant peak near 19 kHz being due to the first bending mode resonance of the copper dome. There is no discernible frequency response deviation in moving from voltage drive to current drive with this device, due to its high level of intrinsic damping.

While the low-frequency drive unit benefits sub-

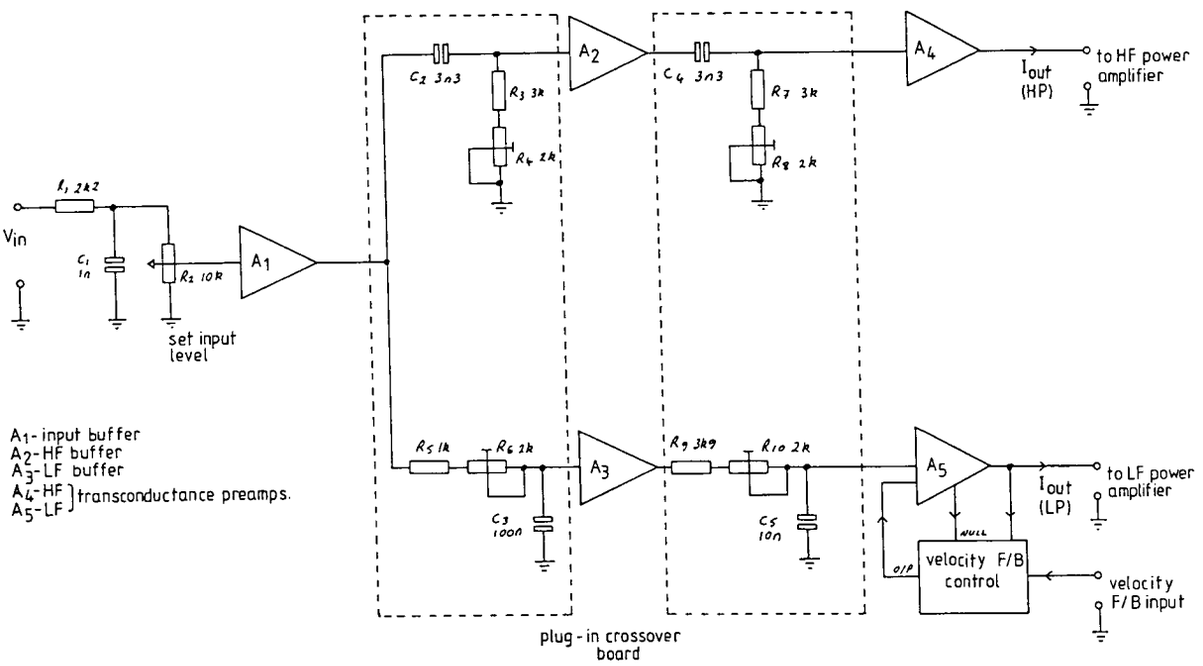

Fig. 18. Block diagram of low-level crossover.

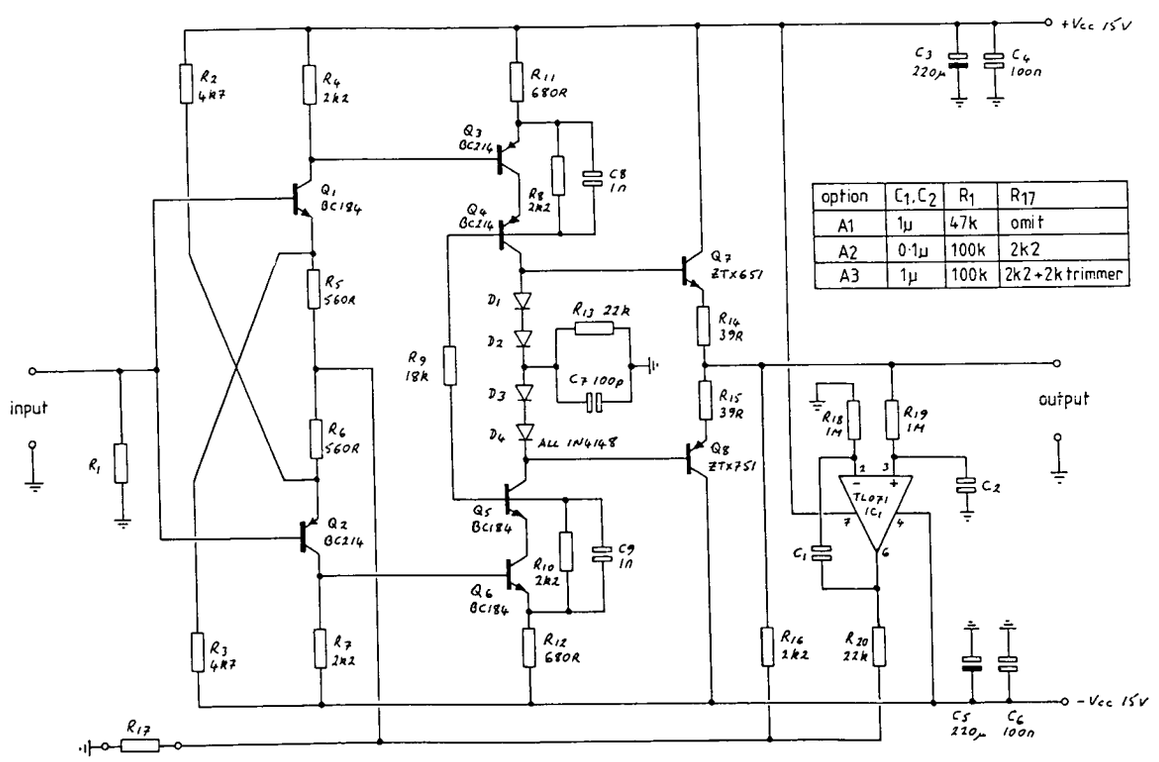

Fig. 19. Buffer amplifiers for crossover network.

stantially from current drive, the improvements in linearity to the tweeter are more modest, largely as a result of a more linear magnetic circuit and lower cone displacements. A distortion improvement of typically 3–7 dB is afforded. However, benefits in terms of the elimination of thermally induced errors are still apparent.

5 DYNAMIC CURRENT AND VOLTAGE DEMAND

Under certain signal conditions, drive units and loudspeaker systems have, under voltage drive, been shown to exhibit an instantaneous impedance modulus lower than might initially be suggested from the steady-state impedance characteristics, thus stressing the power amplifier in terms of current delivery [24]–[28]. In this section we consider the implications of this work in relation to current drive.

As an example, the bass–midrange unit and enclosure combination is considered. The equivalent electrical model is shown in Fig. 21. Under voltage drive, a pulse is applied to the drive unit, the duration of which is set to excite the large negative-going current excursion shown in Fig. 22. The voltage signal has been second-order low-pass filtered at 3 kHz to represent realistic operating conditions. At the point of maximum negative-going current, the instantaneous impedance modulus is 4.15 Ω, lower than the steady-state minimum of 7 Ω.

Under current drive it is only realistic to consider the drive unit when equalized by velocity feedback to give the same Q at fundamental resonance as in the voltage-driven case ($Q \approx 0.7$). Under these conditions, also with a 3-kHz crossover point, the current waveform is seen to be similar to the voltage-driven case, while the voltage waveform shows peaks due to the voice-coil inductance (Fig. 23). The instantaneous impedance modulus is similar to that under voltage drive, but slightly lower at 4.05 Ω.

The main significance of these results is that while the power amplifier is similarly stressed under both voltage and current drive, allowance must be made for sufficient headroom in the power amplifier for the voltage peak resulting from the coil inductance. The problem is worsened by voice-coil heating. The effect of a temperature rise of 200°C (meaning that the coil resistance increases to 13 Ω using copper) is shown by the waveforms of Fig. 24. While the current waveform is identical to that at normal temperature, as expected, the voltage waveform is increased in magnitude in order to keep the current constant. The negative-going excursion is seen to be 1.7 times greater. Although the performance of the drive unit is unaffected by the in-

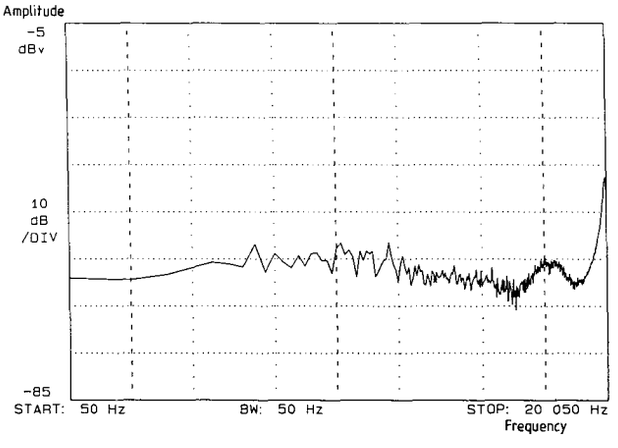

Fig. 20. Measured frequency response of complete system.

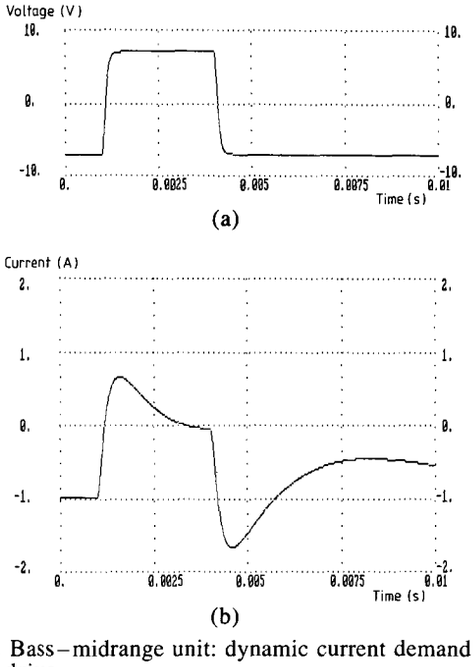

Fig. 22. Bass–midrange unit: dynamic current demand under voltage drive.

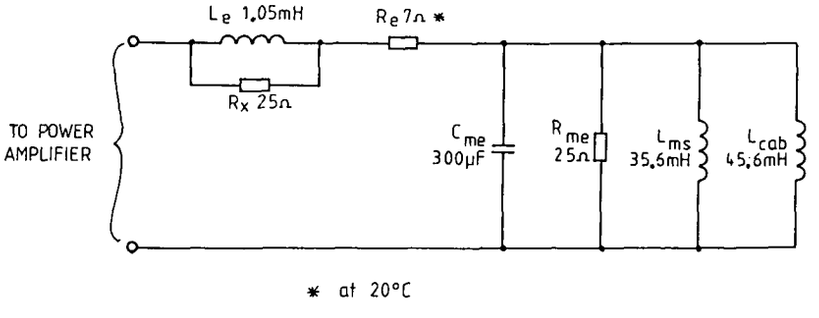

Fig. 21. Electrical model of bass–midrange drive unit and enclosure combination. L_e—voice-coil inductance; R_x—losses due to pole piece coupling; R_e—voice-coil resistance; C_{me}—capacitance due to moving mass; R_{me}—resistance due to mechanical losses; L_{ms}—inductance due to suspension compliance; L_{cab}—inductance due to volume of air in cabinet.

creased temperature, care must be taken in selecting the supply voltages for the power amplifier to avoid voltage clipping, with implications regarding the safe operating area of power devices.

6 CONCLUSIONS

In this paper we have considered a prototype two-way active current-driven loudspeaker system. The main benefits of current drive are seen to be a freedom from thermally induced distortion effects and also high-frequency nonlinearity caused by the voice-coil inductance.

By reviewing earlier work on transconductance power amplifiers, the limitations of these approaches were noted and a novel topology described, employing a common-base isolating stage to drive the loudspeaker. This decouples the nonlinear load from the feedback loop of the amplifier and provides a naturally high output impedance. For low-frequency operation, motional feedback is acknowledged as providing a suitable method of damping the drive unit fundamental resonance. A velocity-sensing coil was employed for this purpose, wound over the main driving coil, with electronic compensation used to null the transformer coupling error between the two. At high frequencies, where motional feedback is no longer feasible, a drive unit with good self-damping properties is recommended, although open-loop compensation could also be considered.

While the power amplifier circuits presented may be regarded as being somewhat complicated, they demonstrate some of the earlier work carried out within the group on distortion correction techniques. The availability of new hybrid gain stage devices (such as the Deltec DH-OA32) with high open-loop bandwidth and good output voltage and current-driving capabilities considerably simplifies the task of power amplifier design.

The provision of velocity feedback control circuitry introduces additional complexity over voltage drive, but this must be considered the price to be paid for what is regarded as a most worthwhile improvement in loudspeaker performance.

7 REFERENCES

[1] M. R. Gander, "Dynamic Linearity and Power Compression in Moving-Coil Loudspeakers," presented at the 76th Convention of the Audio Engineering Society, *J. Audio Eng. Soc. (Abstracts)*, vol. 32, pp. 1008–1009 (1984 Dec.), preprint 2128.

[2] J. R. Gillion, P. L. Boliver, and L. C. Boliver, "Design Problems of High-Level Cone Loudspeakers," *J. Audio Eng. Soc. (Project Notes/Engineering Briefs)*, vol. 25, pp. 294–299 (1977 May).

[3] T. S. Hsu, S. H. Tang, and P. S. Hsu, "Electromagnetic Damping of High-Power Loudspeakers," presented at the 79th Convention of the Audio Engineering Society, *J. Audio Eng. Soc. (Abstracts)*, vol. 33, p. 1011 (1985 Dec.), preprint 2297.

[4] W. J. Cunningham, "Nonlinear Distortion in Dynamic Loudspeakers Due to Magnetic Effects," *J. Acoust. Soc. Am.*, vol. 21, pp. 202–207 (1949 May).

[5] J. A. M. Catrysse, "On the Design of Some

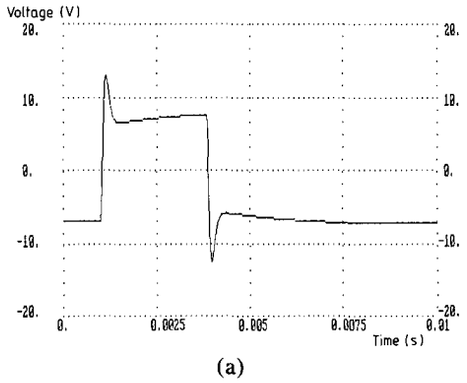

(a)

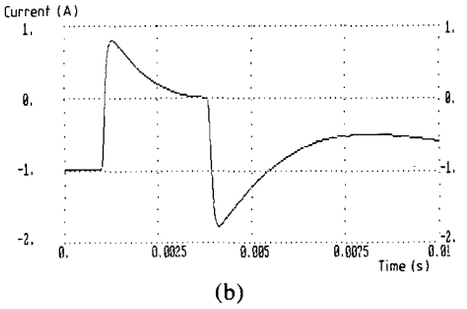

(b)

Fig. 23. Dynamic excitation under current drive.

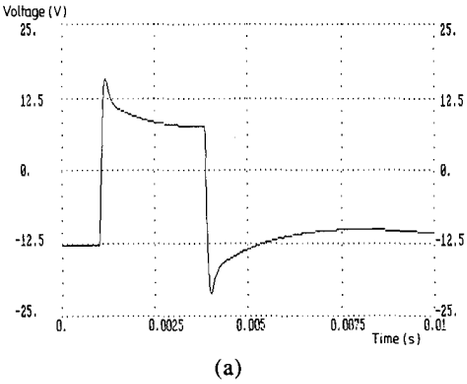

(a)

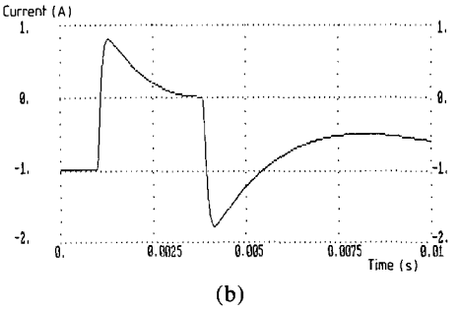

(b)

Fig. 24. Dynamic excitation as for Fig. 23, but voice-coil temperature raised to 200°C (R_e = 13 Ω).

Feedback Circuits for Loudspeakers," presented at the 73rd Convention of the Audio Engineering Society, *J. Audio Eng. Soc. (Abstracts)*, vol. 31, p. 364 (1983 May), preprint 1964.

[6] R. A. Greiner and T. M. Sims, Jr., "Loudspeaker Distortion Reduction," *J. Audio Eng. Soc.*, vol. 32, pp. 956–963 (1984 Dec.).

[7] K. Lewis, "Transconductance Amplifiers," *Electron. Wireless World*, pp. 580–582 (1987 June).

[8] A. Nedungadi, "High Current Class AB Converter Technique," *Electron. Lett.*, vol. 16, pp. 418–419 (1980 May).

[9] M. K. N. Rao and J. W. Haslett, "Class AB Voltage-Current Converter," *Electron. Lett.*, vol. 14, pp. 762–764 (1978 Nov.).

[10] M. J. Hawksford, "Low-Distortion Programmable Gain Cell Using Current-Steering Cascode Topology," *J. Audio Eng. Soc.*, vol. 30, pp. 795–799 (1982 Nov.).

[11] E. H. Nordholt, *Design of High-Performance Negative-Feedback Amplifiers* (Elsevier, Amsterdam, 1983).

[12] J. J. Davidson, "A Low-Noise Transistorized Tape Playback Amplifier," *J. Audio Eng. Soc.*, vol. 13, pp. 2–16 (1965 Jan.).

[13] J. L. Linsley Hood, "Symmetry in Audio Amplifier Circuitry," *Electron. Wireless World*, pp. 31–34 (1985 Jan.).

[14] R. N. Marsh, "A Passively Equalised Phono Pre-amplifier," *Audio Amateur*, no. 3, pp. 18 (1980).

[15] M. Hawksford, "Reduction of Transistor Slope Impedance Dependent Distortion in Large-Signal Amplifiers," *J. Audio Eng. Soc.*, vol. 36, pp. 213–222 (1988 Apr.).

[16] M. J. Hawksford, "Power Amplifier Output-Stage Design Incorporating Error-Feedback Correction with Current-Dumping Enhancement," presented at the 74th Convention of the Audio Engineering Society, *J. Audio Eng. Soc. (Abstracts)*, vol. 31, p. 960 (1983 Dec.), preprint 1993.

[17] P. G. A. H. Voight, "Improvements in or Relating to Thermionic Amplifying Circuits for Telephony," *UK patent 231972* (1924 Jan.).

[18] J. A. Klaassen and S. H. de Koning, "Motional Feedback with Loudspeakers," *Philips Tech. Rev.*, vol. 29, pp. 148–157 (1968).

[19] D. de Greff and J. Vandewege, "Acceleration Feedback Loudspeaker," *Wireless World*, pp. 32–36 (1981 Sept.).

[20] G. J. Adams, "Adaptive Control of Loudspeaker Frequency Response at Low Frequencies," presented at the 73rd Convention of the Audio Engineering Society, *J. Audio Eng. Soc. (Abstracts)*, vol. 31, p. 364 (1983 May), preprint 1983.

[21] E. de Boer, "Theory of Motional Feedback," *IRE Trans. Audio*, pp. 15–21 (1961 Jan./Feb.).

[22] A. F. Sykes, "Damping Electrically Operated Vibration Devices," *UK patent 272622* (1926 Mar.).

[23] R. L. Tanner, "Improving Loudspeaker Response with Motional Feedback," *Electronics*, pp. 142 ff. (1951 Mar.).

[24] P. G. L. Mills and M. J. Hawksford, "Transient Analysis: A Design Tool in Loudspeaker Systems Engineering," presented at the 80th Convention of the Audio Engineering Society, *J. Audio Eng. Soc. (Abstracts)*, vol. 34, p. 386 (1986 May), preprint 2338.

[25] I. Martikainen, A. Varla, and M. Otala, "Input Current Requirements of High-Quality Loudspeaker Systems," presented at the 73rd Convention of the Audio Engineering Society, *J. Audio Eng. Soc. (Abstracts)*, vol. 31, p. 364 (1983 May), preprint 1987.

[26] M. Otala and P. Huttunen, "Peak Current Requirement of Commercial Loudspeaker Systems," *J. Audio Eng. Soc.*, vol. 35, pp. 455–462 (1987 June).

[27] D. Preis, "Peak Transient Current and Power into a Complex Impedance," presented at the 80th Convention of the Audio Engineering Society, *J. Audio Eng. Soc. (Abstracts)*, vol. 34, p. 386 (1986 May), preprint 2337.

[28] J. Vanderkooy and S. P. Lipshitz, "Computing Peak Currents into Loudspeakers," presented at the 81st Convention of the Audio Engineering Society, *J. Audio Eng. Soc. (Abstracts)*, vol. 34, pp. 1036–1037 (1986 Dec.), preprint 2411.

Biographies for Drs. Mills and Hawksford were published in the March issue.